Title
Technical report: the design and evaluation of a basin-scale wireless sensor network for mountain hydrology

Permalink
https://escholarship.org/uc/item/6b8846ff

Authors
Zhang, Ziran
Glaser, Steven D
Bales, Roger C
et al.

Publication Date
2017

Peer reviewed

Technical report: the design and evaluation of a basin-scale wireless sensor network for mountain hydrology

Ziran Zhang[1], Steven D. Glaser[1], Roger C. Bales[1,2], Martha Conklin[2], Robert Rice[2] and Danny G. Marks[3]

[1]Department of Civil and Environmental Engineering, University of California, Berkeley
[2]Sierra Nevada Research Institute and School of Engineering, University of California, Merced
[3]Agricultural Research Service, USDA, Boise

Key Points:
- This first basin-scale wireless-sensor network provides reliable, representative measurements in a mountain basin.
- The distributed network better characterizes patterns of key hydrologic variables compared to operational networks
- Used with spatially explicit modeling and other spatial data, the network offers unprecedented opportunities for improved hydrologic prediction

---

Abstract

A network of sensors for spatially representative water-balance measurements was developed and deployed across the 2000 km^2 snow-dominated portion of the upper American River basin, primarily to measure changes in snowpack and soil-water storage, air temperature and humidity. This wireless sensor network (WSN) consists of 14 sensor clusters, each with 10 measurement nodes that were strategically placed within a 1-km^2 area, across different elevations, aspects, slopes and canopy covers. Compared to existing operational sensor installations, the WSN reduces hydrologic uncertainty in at least three ways. First, redundant measurements improved estimation of lapse rates for air and dew-point temperature. Second, distributed measurements captured local variability and constrained uncertainty in air and dew-point temperature, snow accumulation and derived hydrologic attributes important for modeling and prediction. Third, the distributed relative-humidity measurements offer a unique capability to monitor upper-basin patterns in dew-point temperature and characterize elevation gradient of water vapor-pressure deficit across steep, variable topography. Network statistics during the first year of operation demonstrated that the WSN was robust for cold, wet and windy conditions in the basin. The electronic technology used in the WSN reduced adverse effects, such as high current consumption, multipath signal fading and clock drift, seen in previous remote WSNs.

Index Terms and Keywords: Wireless-sensor network, water-information system, snow observation, mountain hydrology, Sierra Nevada.

1 Introduction

Currently, in situ measurements of mountain water cycles at the basin scale are limited in both spatial coverage and temporal resolution, with data largely provided by a relatively small number of operational precipitation, snowpack, climate and stream-gauging stations [*Bales et al.*, 2006; *Dozier*, 2011]. In the Sierra Nevada, measurement sites supporting operational water-resources decision making are also biased to middle and lower elevations and flat terrain in forest clearings [*Molotch and Bales*, 2005].

Hydrologic prediction, particularly when constrained by the practical demands of water-resources management, relies heavily on calibrated models to mitigate both limitations in model formulation and inadequate data for rigorous model testing [*Kuczera et al.*, 2010; *Semenova and Beven*, 2015]. There are increasing demands on distributed models as predictive tools for situations in which lumped models may fall short, such as non-stationarity in catchment conditions or climate; however, their use in water-resources management is limited by the level of field data available [*Refsgaard*, 1997]. The need for improved coverage by in situ measurements is both local and global, and new network designs should complement satellite data [*Wood et al.*, 2011]. Ground-based sensors provide critical ground truth for remotely sensed satellite and aircraft data, and offer a wide

suite of independent data that can help provide much-needed gains in predictive modeling. Realizing gains in accuracy from the next generation of spatially explicit models at the scale of water-resources decision making will require both the broad spatial coverage of remotely sensed data and the accuracy of in situ measurements [*Lehning et al.*, 2009]. An adaptive rather than one-size-fits-all approach is needed to realize these gains [*Fenicia et al.*, 2008].

Wireless Sensor Networks (WSNs) are an efficient and economical solution for distributed sensing. It is often costly and disruptive to create networks of spatially representative wired sensors at the scale desired since it might require kilometers of cables placed either above ground or buried. Similarly, access to data for distributed sensors with only local logging is limited by the need to visit sites to download data. Reliable wireless solutions are now enabled by reduced production costs of wireless equipment and by advances in networking protocols, effectively combining traditionally wired sensors with a wireless platform. [*Akyildiz et al.*, 2002; *Yick et al.*, 2008; *Gilbert*, 2012].

A few WSN solutions, using different network technologies, were developed specifically for applications in hydrology. These studies have not provided quantifiable assessments of network design, operation and hydrologic results at the river-basin scale. A review of these prior deployments, and a comparison of three existing WSN solutions that have been used, is provided in supporting information (See text S1) [*Digi*, n.d.; *Bogena et al.*, 2010; *Pister and Doherty*, 2008; *Gungor and Hancke*, 2009; *International*, 2009; *Ritsema et al.*, 2010; *Simoni et al.*, 2011; *Horvat*, 2012; *Huang et al.*, 2012; *Kerkez et al.*, 2012; *Accettura and Piro*, 2014; *Pohl et al.*, 2014; *ZigBee*, 2009].

While sensor networks deployed in headwater catchments for short durations offer lessons for local-scale WSNs, they provide limited guidance for WSN design, performance and hydrologic benefits for systems in larger mountain river basins, characterized by steep gradients in temperature, precipitation, rain-versus-snow fraction, growing season, vegetation density and evapotranspiration. The proposed approach to scaling WSN measurements to larger basins involves strategically placing local clusters to capture the variability in hydrologically important basin attributes [*Welch et al.*, 2013].

The aim of the research described in this technical report was to develop a flexible, robust method for measurement of the spatial water balance across a seasonally snow-covered mountain basin. In doing this, we addressed three questions. First, to what extent can a basin-scale distributed wireless-sensor network with a limited number of sensors arrayed in local clusters sample hydrologic variables across a representative range of landscape attributes in a seasonally snow-covered mountain basin? Second, to what extent can this low-power, distributed wireless-sensor network reliably provides hydrologic data during harsh winter conditions? Third, what types of gains in hydrologic information may result from this network? Further development and more-detailed analysis of the third question is also the subject of subsequent analysis.

2 Methods

The network was deployed in the American River Hydrologic Observatory (ARHO), in the upper, snow-dominated portion of the American River basin on the western slope of the Sierra Nevada in California (36.069 N, -120.583 W). The basin is incised with steep river canyons and is comprised of three sub-basins: the North, Middle, and South forks, which combine to form a drainage basin of 5311 km^2 above the Folsom Reservoir, the main impoundment on the river (Fig. 1a). Basin elevations range from 15 m at Folsom to 3147 m at the Sierra crest, with precipitation transitioning from rain to snow at about 1400-1600 m elevation [*Raleigh and Lundquist*, 2012; *Klos et al.*, 2014]. Forty percent, or about 2000 km^2, of the basin is above 1500 m, the lowest elevation for siting our WSNs. About 0.5% of the basin is above the highest node that was sited (2678 m).

In 2013-2015, 14 clusters of wireless nodes were deployed (Fig. 1a), with locations selected to represent the range of elevation, aspect, canopy coverage, and solar loading in the basin (Fig. 1b and S1). Each node had a number of sensors, as described in Supporting Information; with air temperature, relative humidity and snow depth the subject of this report. The number of local clusters was based on results of Welch et al. [2013], and constrained by project budget. The Welch et al.

analysis used spatial time-series data over 11 years and a rank-based clustering approach to identify measurement locations that will be most informative for real-time estimation of snow depth, and derived a set of regions that remained relatively stable over time. They found a point of marginal return at about 15 measurement locations, after which placing more local sensor networks did not significantly improve estimation performance. The Welch et al. study also showed that there is some flexibility in placing the local clusters to capture representative parts of the basin, and thus all sites, except MTL and DOR, were co-located with existing snow pillows and met stations. Each cluster consists of ten measurement nodes, limited due to budget, seven to 35 signal-repeater nodes, and a network manager (see Table S1 for details; and Fig. S2 for system hierarchy).

Measurement-node placement consisted of three steps. First, major physiographic variables that affect snow distribution, and by extension other components of the water balance, were characterized in a 1-km^2 area around each site [*Balk and Elder*, 2000; *Erxleben et al.*, 2002; *Anderton et al.*, 2004; *Essery and Pomeroy*, 2004; *Sturm and Benson*, 2004; *Erickson et al.*, 2005; *Marchand and Killingtveit*, 2005; *Bales et al.*, 2006]. Second, at each site ten points representing different physiographic attributes were selected by a random-stratified technique, and the attributes aggregated to assess their representativeness in the larger basin (See text S2 [*Jin et al.*, 2013]). Rice and Bales [2010] showed that a 10-sensor network could capture the mean and distribution of snow depths at this scale. Third, final location adjustments were made in the field to a small subset of sensor nodes, ensuring a complete sampling of the physiographic features together with a strong WSN connection mesh. See Supporting Information for node details (Text S3).

The network statistics presented were evaluated over a period of 7 months. Each node provided 15-minute data for snow depth, air temperature and relative humidity. Hourly and daily products were developed for periods where no less than 75% of data were present and valid within the averaging window. Extreme values in the data were removed following *Daly et al.* [2008]. Operational data were downloaded from the California Department of Water Resources (http://cdec.water.ca.gov/). Data from SNODAS, a gridded national operational product that is developed from weather-forecast and snowmelt models, plus ground-based and remotely sensed data, were used as an additional point of comparison with our snow measurements (http://nsidc.org/data/). Hourly dew-point temperature for each node was computed based on an empirical equation [*Lawrence*, 2005].

3 Results

3.1 WSN performance

The wireless-network links formed a redundant multi-hopped mesh network of sensors and repeaters for data transport. Fig. 2 shows the stable layout of sensor nodes for the Alpha cluster (ALP), and illustrates how repeaters were non-uniformly distributed to connect the sensor nodes via at least two independent paths to the base station (see Fig. S5 for photographs of base station, nodes and repeater). During 213 days of consecutive recording only 662 out of over 56 million packets were lost in transmission. The average number of hops for packets to transmit from a node to the base station was 3.6 and the maximum seven. The average latency of the network, the time it takes from the packet being sent until it arrived at the base station, was 1.01 second. On average, each node received 181,000 packets over the period when network statistics were gathered.

Two measures indicate the reliability and performance of the network: i) the number of other sensor or repeater nodes connected to each node and ii) the average received signal strength indicator (RSSI). RSSI is closely associated with an important network-performance indicator called packet delivery ratio (PDR). In aggregate, each node was connected to at least two other nodes over 95% of the time, and to three or more nodes 68% of the time (see Fig. S6). Taking all nodes together, RSSI values were above -85 dBm, the manufacturer-specified threshold for efficient transmission over 54% of the time, with values above -80 dBm 33% of the time.

Environmental factors have been thought to impact the performance of WSNs [*Boano et al.*, 2010; *Marfievici et al.*, 2013]. For our local clusters there was no clear influence of environmental factors, e.g., temperature, humidity and snow-induced topographic changes, on network performance (Fig. 3). Each node was connected to one to five other nodes at each time step (Fig. 3a). RSSI values at each node typically fluctuated ±5

dBm, and the average RSSI (Fig. 3b) depended on node location as opposed to temperature (Fig. 3c), humidity (Fig. 3d) or topographic changes due to snow accumulation (see water-year days 72 and 80, Fig. 3e). It was discovered that absolute topography influenced connectivity.

3.2 Temperature, humidity and snow patterns

Daily air and dew-point temperatures from the 10 wireless-sensor clusters that were installed prior to the 2014 water year showed very similar temporal patterns (Fig. 4a), with average temperature differences reflecting elevation differences between clusters. Temperatures for all pairs of clusters were highly correlated, r > 0.91 for air temperature and r >0.86 for dew-point temperature, p < 0.05.

Daily temperatures were used to derive surface-level lapse rates, which over the eight-month period varied from close to zero to -12ºC/km for both air and dew-point temperatures (Fig. 4b). The respective average lapse rates for the months before snow accumulation (Oct-Dec) were -4.6 and -5.7 ºC/km, increasing to -5.5 ºC/km for air temperature and decreasing to -4.7 ºC/km for dew-point temperature during the snow season. The day-to-day variability in lapse rates during the snow-covered period was also lower than earlier in the water year. The transition to a period with less variability in lapse rate is also illustrated by the higher R^2 values starting on water-year day 121, when snow started accumulating in the basin (Fig 4c). Note that less-negative air-temperature lapse rates, associated with lower R^2 values, were associated with temperature inversions.

Daily mean air and dew-point temperatures taken across the ten clusters were adjusted to 2100 m using the mean daily lapse rates (Fig. 4d). The average standard deviation is 3.3 ºC for air temperature and 3.5 ºC for dew-point temperature, a variability equivalent to the average difference over about 600 m and 545 m elevation based on the eight-month average lapse rate of -5.5 ºC/km and -5.0 ºC/km, respectively. While any index elevation could be used for this comparison, 2100 m is generally representative of the upper part of the rain-snow-transition elevation zone.

Mean relative humidity across WSN clusters varied from 15 to 100%, with similar patterns across all 10 clusters (Fig. 4e). The correlations were strong, r = 0.91, p < 0.05, for all pairs of clusters. Differences in absolute humidity and vapor-pressure deficit between clusters were in some cases relatively large. The mean water vapor-pressure deficit for each cluster ranged from zero to 1.5 kPa (Fig. 4f), with daily inter-cluster differences between the lowest and highest values as much as 55%. The highest variability in vapor-pressure deficit was associated with periods of higher temperature and lower relative humidity, indicating a warmer and drier condition. Periods with lower variability of inter-site vapor-pressure deficit were closely associated with sub-zero temperatures in the basin, typically triggered by precipitation events.

Snow-depth data (Fig. 5) show a clear elevation trend, with variability also increasing with elevation. One exception was SCN, which has a tighter grouping of measured snow depths as compared to lower-elevation sites. During the very warm and dry WY-2014 snow season, sustained snow cover accumulated mainly at elevations above 2100 m.

Snow depths were also compared with co-located or nearby snow-course measurements (Fig. 5). At lower-elevation clusters, due to the timing of the snow-course measurements, most surveys missed the snow-cover peak accumulation. At ONN, snow-course data showed a small amount of snow throughout the season, missing the few individual peaks. Snow-course values at ECP were generally lower than the mean cluster value across the season.

There were substantial differences between the WSN, nearby operational snow-depth sensors, and SNODAS snow depth at most clusters. Compared to WSN means, nearby operational sensors tended to overestimate snow depth during early season (e.g. at ECP, CAP, and ALP), and better matched the WSN mean at peak accumulation. Nearby operational sensors also showed faster melt than indicated by cluster means for the same sites. The time series of SNODAS values is comparable to the WSN data at MTL and SCN for much of the season, with similar magnitude and high correlation. SNODAS data generally fall within one standard deviation of WSN nodes at these sites. At lower-elevation sites, such as BTP, VAN and DUN, SNODAS underestimated snow depth at peak accumulation by as much as 50% compared to the WSN. At all other sites, SNODAS overestimated peak-accumulation snow depth by as much as 80% compared to the WSN mean.

4 Discussion

4.1 WSN design and performance

With 555 sensors across 14 clusters, the WSN offers representative, real-time monitoring of the meteorological and hydrologic conditions of much of the upper reaches of the basin. The size of this network, arguably the largest long-term, remote wireless-sensor platform deployed for environmental monitoring, shows that WSNs are now capable of being used for major instrumentation projects. Even though some aspects of the networks in ARHO share similar properties with the prototype installation at the Southern California Critical Zone Observatory [*Kerkez et. al*. 2012], the more-recent network statistics help to resolve several previously unanswered networking questions important to the broader wireless communications community as well as to field hydrologists. The longer-term performance of the networks, subjected to the test of a full snow season, showed that WSNs can be a viable solution for distributed sensing at this scale. ARHO networks showed resilience to factors such as humidity and snow-induced topographic changes across different part of the basin. The positive result is likely due to the combination of the Dust Network's radio technologies such as time-synchronized channel-hopping, time-slotted mesh protocol (see section S1.2.3 for details of the technology), effective network topology, and the use of lower-gain antennas.

A stringent criterion of design was low power consumption, requiring the sensor node to be powered with a 6-amp-hour battery recharged by a 10-watt solar panel. The low-power requirement constrains radio-power output, so the range of the radio limits the size and performance of the network. Through iterative design and careful control over circuitry we were able to attain our goal. The final design is basically two very low-power-consumption microchips – a Cypress PSoC5 and Dust networks radio module. This is useful to the community, which by and large uses systems based on technology that has 100 or more times the power consumption (see Supporting Information).

Topographic relief is one of the more-serious challenges to overcome for good system performance. Different from earlier installations, the networks in ARHO encountered more-challenging, steep forested terrain. A lower-gain 4-dBm gain omni-directional antenna provided improved network connectivity due to its "fatter" radiation pattern, especially in steep terrain, compared to the 12-dBm gain antennas used by Kerkez et al [2012] on more-even terrain. Even with the improvement, the capability of the network to communicate over steep slopes is limited by the antenna. The ALP site is a good example of where some radio links operated at the edge of the acceptable RSSI level due to steep topography. A relatively large number of repeaters were installed to provide redundant paths to sensor nodes 6, 8, and 9, where a steep change in slope produced a radio path "kink" and reliable network links were challenging to establish. The network performance was stable but less efficient, indicated by the lower PDR values, compared to *Kerkez et al.* [2012], who had shorter data hops.

4.2 Spatial pattern and variability of hydrologic attributes

The following three examples illustrate how our spatially distributed, daily data over complex terrain set provides improved estimates of important hydrologic attributes, compared to less-dense operational measurements. A more-detailed analysis will be the subject of a subsequent report.

4.2.1 Air and dew-point temperature. A widely accepted model of near-surface air temperature in mountains is the ground-level lapse rate [*Dodson and Marks*, 1997; *Rolland*, 2003; *Huang et al.*, 2008; *Kirchner et al.*, 2013]. Scientists and modelers use lapse-rate-derived temperature to evaluate model responses due to temperature perturbations [*Gardner and Sharp*, 2009; *Bales et al.*, 2015]. In those applications the lapse rate, often averaged over a monthly to annual period, is used to approximate input temperature for models with a much shorter (daily) time increment. This approach, however, does not account for short-term variability. WSN data show that the day-to-day lapse rate was highly variable, particularly before snow accumulation (Fig. 4b). Not only does the array of sensors provide a more temporally resolved lapse-rate estimate, we also found that the redundancy of sensors provides a more-robust estimate of the amplitude. Linear models of daily air temperature were constructed with a training set and a cross-validation set of 60 randomly selected nodes. The results were compared with models computed using seven nearby met stations. On average, the cross-

validation root-mean-square error was reduced from 1.4 to 1.2 °C using random sets of 60 measurements versus data from seven nearby met stations. The uncertainty in air temperature was reduced by 16%.

A one-way analysis of variance (ANOVA) analysis was done for a 20-day period around the time of peak snow accumulation to assess within-cluster versus between-cluster variability. On average, over 85% of the variability in daily air temperature is between clusters, with a peak within-cluster variability of 24% (Fig. 6a). The within-cluster variation can be more significant at night, as seen by the pattern in the hourly data, when up to 40% of the variability was within cluster. We also considered the difference between daily temperatures for operational sites versus cluster values. Comparing sensor-node values for nodes that have the same landscape features as do operational measurements (flat, open) versus other nodes shows a 0.8°C difference for one site, and 0-0.3°C for five other sites; however the values are not different at the 95% confidence level (Figure S8a).

Dew-point temperature complements air temperature in providing a reliable estimate of the timing and phase of precipitation. The reduction of uncertainty in temperature and humidity patterns helps to better determine the elevation range of the rain/snow transition. Air temperature is approximately equal to dew-point temperature, indicating saturated air, when precipitation occurs (Fig. 4). The phase change from rain to snow usually occurs around the 0°C dew-point [*Marks et al.*, 2013]. Compared to air-temperature-based methods, dew-point temperature is a less geographically dependent variable to determine the solid or liquid precipitation [*Ye et al.*, 2013]. Due to lack of relative-humidity measurements for most met stations, calculation of dew-point temperature cannot be performed from met-station data alone.

Feld et al. [2013] assessed various methods of estimating daily dew point, and found that a weather-forecast model that captured some aspects of local topography provided less-biased estimates than did simpler constant-lapse-rate or constant-humidity approaches. Their median dew-point lapse rate, based on 15 met stations and 35 hygrochons deployed in the North Fork American basin and averaged over 3 years, was -5.3 °C/km, comparable to our mean of -5.0 °C/km. However, our -5.5 °C/km mean air-temperature lapse rate was smaller than their 3-year average of -6.3 °C/km. More extensive analysis of our seasonal and spatial patterns will be the subject of a subsequent report.

4.2.2. Evaporative potential. Direct measures of vapor-pressure-deficit patterns from a dense array of ground-based sensors can be important for scaling evapotranspiration and assessing forest health [*Oren et al.*, 1999, 2001; *Bowling et al.*, 2002]. Accurately estimating vapor-pressure deficit is crucial as the saturation-pressure deficit becomes relatively more important in the Penman-Monteith equation [*Ziemer*, 1979]. Despite the importance of the variable, reliable field-based estimates of vapor-pressure deficit in mountains are rare. The performance of satellite-based estimates varies, with RMSE values from upwards of 0.3 kPa to 1.1 kPa, limiting their accuracy as estimates of vapor-pressure deficit across steep terrain [*Prince et al.*, 1998; *Hashimoto et al.*, 2008]. A WSN with relative-humidity measurement at every sensor node fills this gap.

The ANOVA results for daily relative humidity are similar to those for temperature, with most of the variance being between versus within clusters (Fig. 6b). There was, however, no clear day-night pattern. In addition, there were only small differences in humidity between nodes that represent the varying landscape attributes of operational sensors, versus values for other nodes. One of the 6 sites evaluated had a significant difference, reflecting in large part the temperature differences (Figure S8b).

4.2.3 Snow depth. The differences in snow depth between WSN and nearby operational sensors can be explained by the patterns of snow accumulation. Operational snow-depth sensors are typically placed near flat meadows or ridge tops free of overhead obstructions or hazards, which produce known biases [*Molotch and Bales*, 2006; *Ainslie and Jackson*, 2010; *Rice and Bales*, 2010]. We placed our nodes in both forested and non-forested area to produce a more spatially representative measurement. Fig. 5 indicates that operational snow-depth sensors data had a systematic positive bias in snow depth in the early season. During the melting season, the canopy acts as a shield, limiting energy input to the snowpack [*Marks et al.*, 1998; *Sicart et al.*, 2004; *Pomeroy et al.*, 2012]. The canopy also shelters the snow surface from wind, reducing turbulent heat transfer. The net result is an extended melt season recorded by sensor nodes in

the forested area compared to the operational snow-depth sensors.

The ANOVA results for daily snow depth show that both within-cluster and between-cluster variability to be important. About 60% of the variability was between clusters and 40% within clusters immediately after the accumulation event ending on water-year day 183, with both values converging toward 50% over the next 2 weeks. Comparing nodes having landscape attributes like those of operational sites (flat, open) versus other nodes also shows relatively large within-cluster differences between the two sets at most of the six sites evaluated (Figure S8c).

Due to local redundancy of the WSN, the data stream is more complete than operational snow-depth sensors at CAP and BTP. Large sections of data were missing from the operational-snow-depth sensors from those two sites during the storm around water-year day 180 (Fig. 5). This reflects a reality of operational water-resources networks, namely the inability to respond in a timely manner to problems in remote sensors. The redundancy provided by our WSNs helps to address this constraint.

The differences in snow depth between SNODAS and the WSN were less systematic, as there is no apparent trend in the bias across different sites. One pronounced difference between WSN and SNODAS snow depth was at the steep ECP site, where the 1-km^2 SNODAS product overestimated snow depth compared to our measurements (Fig. 5). This follows previous reports that without sufficient data, estimates of snow depth under these conditions can be difficult and error prone due to the underlying variance in elevation within grid boundaries [*Hedrick et al.*, 2015]. *Clow et al.* [2012] showed that for over-forested regions of the Colorado Rockies, SNODAS estimates of snow depth accounted for as much as 72% of the variance line (1-km resolution) in forested areas, but SNODAS was only able to account for 16% of snow-depth variance in areas above the treeline.

5 Conclusions

A wireless-sensor network distributed over the 2000 km^2 snow-dominated portion of a mountain basin provided effective coverage of watershed attributes. With ten measurement nodes per each of fourteen clusters, the WSNs reliably provided spatially distributed measurements of temperature, relative humidity and snow depth every 15 minutes over the basin. The WSN also provided measurements of the significant within-cluster spatial variability of these attributes, which were influenced by local topography, possibly through cold-air drainage effects on temperature.

Compared to existing operational sensors, the wireless-sensor network reduces uncertainty in water-balance measurements in at least three distinct ways. Redundant measurements in temperature improved the robustness of temperature lapse-rate estimation, reducing cross-validation error compared to that of using met-station data alone. Second, distributed measurements capture local variability and constrain uncertainty, compared to point measures, in attributes important for hydrologic modeling, such as air and dew-point temperature and snow precipitation. Third, the distributed relative-humidity measurements offer a unique capability to monitor upper-basin patterns in dew-point temperature and better characterize precipitation phase and the elevation of the rain/snow transition.

Acknowledgments

References

Accettura, N., and G. Piro (2014), Optimal and Secure Protocols in the IETF 6TiSCH communication stack, *Proc. IEEE Int. Symp. Ind. Electron.*, doi:10.1109/ISIE.2014.6864831.

Ainslie, B., and P. L. Jackson (2010), Downscaling and bias correcting a cold season precipitation climatology over coastal southern British Columbia using the regional atmospheric modeling system (RAMS), *J.*

Appl. Meteorol. Climatol., *49*(5), 937–953, doi:10.1175/2010JAMC2315.1.

Akyildiz, I., W. Su, Y. Sankarasubramaniam, and E. Cayirci (2002), Wireless sensor networks: a survey, *Comput. Networks*, *38*(4), 393–422, doi:10.1016/S1389-1286(01)00302-4.

Anderton, S. P., S. M. White, and B. Alvera (2004), Evaluation of spatial variability in snow water equivalent for a high mountain catchment, *Hydrol. Process.*, *18*(3), 435–453, doi:10.1002/hyp.1319.

Bales, R. C., N. P. Molotch, T. H. Painter, M. D. Dettinger, R. Rice, and J. Dozier (2006), Mountain hydrology of the western United States, *Water Resour. Res.*, *42*(8), 1–13, doi:10.1029/2005WR004387.

Bales, R. C., R. Rice, and S. B. Roy (2015), Estimated loss of snowpack storage in the Eastern Sierra Nevada with climate warming, *J. Water Resour. Plan. Manag.*, *141*(2), 4014055, doi:10.1061/(ASCE)WR.1943-5452.0000453.

Balk, B., and K. Elder (2000), Combining binary decision tree and geostatistical methods to estimate snow distribution in a mountain watershed, *Water Resour. Res.*, *36*(1), 13–26, doi:10.1029/1999WR900251.

Boano, C. A., N. Tsiftes, T. Voigt, J. Brown, and U. Roedig (2010), The impact of temperature on outdoor industrial sensornet applications, *IEEE Trans. Ind. Informatics*, *6*(3), 451–459, doi:10.1109/TII.2009.2035111.

Bogena, H. R., J. a. Huisman, C. Oberdörster, and H. Vereecken (2007), Evaluation of a low-cost soil water content sensor for wireless network applications, *J. Hydrol.*, *344*(1–2), 32–42, doi:10.1016/j.jhydrol.2007.06.032.

Bogena, H. R., M. Herbst, J. a. Huisman, U. Rosenbaum, a. Weuthen, and H. Vereecken (2010), Potential of wireless sensor networks for measuring soil water content variability, *Vadose Zo. J.*, *9*(4), 1002, doi:10.2136/vzj2009.0173.

Bowling, D. R., N. G. McDowell, B. J. Bond, B. E. Law, and J. R. Ehleringer (2002), 13C content of ecosystem respiration is linked to precipitation and vapor pressure deficit, *Oecologia*, *131*(1), 113–124, doi:10.1007/s00442-001-0851-y.

Clow, D. W., L. Nanus, K. L. Verdin, and J. Schmidt (2012), Evaluation of SNODAS snow depth and snow water equivalent estimates for the Colorado Rocky Mountains, USA, *Hydrol. Process.*, *26*(17), 2583–2591, doi:10.1002/hyp.9385.

Daly, C., M. Halbleib, J. I. Smith, W. P. Gibson, M. K. Doggett, G. H. Taylor, and P. P. Pasteris (2008), Physiographically sensitive mapping of climatological temperature and precipitation across the conterminous United States, doi:10.1002/joc.

Digi, Digi International (n.d.), XBee/XBee-PRO DigiMesh 2.4 user guide.

Document, Z. (2009), ZigBee RF4CE : ZRC Profile Specification.

Dodson, R., and D. Marks (1997), Daily air temperature interpolated at high spatial resolution over a large

mountainous region, *Clim. Res.*, *8*(1), 1–20, doi:10.3354/cr008001.

Dozier, J. (2011), Mountain hydrology, snow color, and the fourth paradigm, *Eos (Washington. DC).*, *92*(43), 373–374, doi:10.1029/2011EO430001.

Erickson, T. a., M. W. Williams, and A. Winstral (2005), Persistence of topographic controls on the spatial distribution of snow in rugged mountain terrain, Colorado, United States, *Water Resour. Res.*, *41*(4), 1–17, doi:10.1029/2003WR002973.

Erxleben, J., K. Elder, and R. Davis (2002), Comparison of spatial interpolation methods for estimating snow distribution in the Colorado Rocky Mountains, *Hydrol. Process.*, *16*(18), 3627–3649, doi:10.1002/hyp.1239.

Essery, R., and J. Pomeroy (2004), Vegetation and topographic control of wind-blown snow distributions in distributed and aggregated simulations for an arctic tundra basin, *J. Hydrometeorol.*, *5*(5), 735–744, doi:10.1175/1525-7541(2004)005<0735:VATCOW>2.0.CO;2.

Feld, S. I., N. C. Cristea, and J. D. Lundquist (2013), Representing atmospheric moisture content along mountain slopes: Examination using distributed sensors in the Sierra Nevada, California, *Water Resour. Res.*, *49*(7), 4424–4441, doi:10.1002/wrcr.20318.

Fenicia, F., J. J. McDonnell, and H. H. G. Savenije (2008), Learning from model improvement: On the contribution of complementary data to process understanding, *Water Resour. Res.*, *44*(6), doi:10.1029/2007WR006386.

Gardner, A., and M. Sharp (2009), Sensitivity of net mass-balance estimates to near-surface temperature lapse rates when employing the degree-day method to estimate glacier melt, *Ann. Glaciol.*, *50*(1), 80–86, doi:10.3189/172756409787769663.

Gilbert, E. (2012), Research issues in wireless sensor network applications: a survey, *Int. J. Inf. Electron. Eng.*, *2*(5), 702–706, doi:10.7763/IJIEE.2012.V2.191.

Gungor, V. C., and G. P. Hancke (2009), Industrialwireless sensor networks: challenges, design principles, and technical approaches, *IEEE Trans. Ind. Electron.*, *56*(10), 4258–4265, doi:10.1109/TIE.2009.2015754.

Hashimoto, H., J. L. Dungan, M. a. White, F. Yang, A. R. Michaelis, S. W. Running, and R. R. Nemani (2008), Satellite-based estimation of surface vapor pressure deficits using MODIS land surface temperature data, *Remote Sens. Environ.*, *112*(1), 142–155, doi:10.1016/j.rse.2007.04.016.

Hedrick, A., H.-P. Marshall, A. Winstral, K. Elder, S. Yueh, and D. Cline (2015), Independent evaluation of the SNODAS snow depth product using regional-scale lidar-derived measurements, *Cryosph.*, *9*(1), 13–23, doi:10.5194/tc-9-13-2015.

Horvat, G. (2012), Power consumption and RF propagation analysis on, , 222–226.

Huang, P., L. Xiao, S. S. Member, S. Soltani, S. S. Member, M. W. Mutka, and N. Xi (2012), The evolution of MAC protocols in wireless sensor networks: a survey, *IEEE Commun. Surv. Tutorials*, *15*(1), 1–20, doi:10.1109/SURV.2012.040412.00105.

Huang, S., P. M. Rich, R. L. Crabtree, C. S. Potter, and P. Fu (2008), Modeling monthly near-surface air temperature from solar radiation and lapse rate: application over complex terrain in Yellowstone National Park, *Phys. Geogr.*, *29*(2), 158–178, doi:10.2747/0272-3646.29.2.158.

International, D. (2009), XBee ® /XBee-PRO ® RF Modules, *Prod. Man. v1.xEx-802.15.4 Protoc.*, 1–69.

Jin, S., L. Yang, P. Danielson, C. Homer, J. Fry, and G. Xian (2013), A comprehensive change detection method for updating the National Land Cover Database to circa 2011, *Remote Sens. Environ.*, *132*, 159–175, doi:10.1016/j.rse.2013.01.012.

Kerkez, B., S. D. Glaser, R. C. Bales, and M. W. Meadows (2012), Design and performance of a wireless sensor network for catchment-scale snow and soil moisture measurements, *Water Resour. Res.*, *48*(July 2011), 1–18, doi:10.1029/2011WR011214.

Kirchner, M., T. Faus-Kessler, G. Jakobi, M. Leuchner, L. Ries, H.-E. Scheel, and P. Suppan (2013), Altitudinal temperature lapse rates in an Alpine valley: trends and the influence of season and weather patterns, *Int. J. Climatol.*, *33*(3), 539–555, doi:10.1002/joc.3444.

Klos, P. Z., T. E. Link, and J. T. Abatzoglou (2014), Extent of the rain-snow transition zone in the western U.S. under historic and projected climate, *Geophys. Res. Lett.*, 4560–4568, doi:10.1002/2014GL060500.

Kuczera, G., D. Kavetski, B. Renard, and M. Thyer (2010), A limited-memory acceleration strategy for MCMC sampling in hierarchical Bayesian calibration of hydrological models, *Water Resour. Res.*, *46*(7), doi:10.1029/2009WR008985.

Lawrence, M. G. (2005), The relationship between relative humidity and the dewpoint temperature in moist air: A simple conversion and applications, *Bull. Am. Meteorol. Soc.*, *86*(2), 225–233, doi:10.1175/BAMS-86-2-225.

Lehning, M., N. Dawes, M. Bavay, M. Parlange, S. Nath, and F. Zhao (2009), Instrumenting the Earth: next-generation sensor networks and environmental science, in *The Fourth Paradigm: Data-Intensive Scientific Discovery*, pp. 45–51.

Marchand, W. D., and Å.˚ Killingtveit (2005), Statistical probability distribution of snow depth at the model sub-grid cell spatial scale, *Hydrol. Process.*, *19*(2), 355–369, doi:10.1002/hyp.5543.

Marfievici, R., A. L. Murphy, G. Pietro Picco, F. Ossi, and F. Cagnacci (2013), How environmental factors impact outdoor wireless sensor networks: a case study, *Proc. IEEE 10th Int. Conf. Mob. Ad-Hoc Sens. Syst. (MASS '13)*, 565–573, doi:10.1109/MASS.2013.13.

Marks, D., J. Kimball, D. Tingey, and T. Link (1998), The sensitivity of snowmelt processes to climate conditions and forest cover during rain-on-snow: a case study of the 1996 Pacific Northwest flood, *Hydrol. Process.*, *12*(10–11), 1569–1587, doi:10.1002/(SICI)1099-1085(199808/09)12:10/11<1569::AID-HYP682>3.0.CO;2-L.

Marks, D., a. Winstral, M. Reba, J. Pomeroy, and M. Kumar (2013), An evaluation of methods for

determining during-storm precipitation phase and the rain/snow transition elevation at the surface in a mountain basin, *Adv. Water Resour.*, *55*, 98–110, doi:10.1016/j.advwatres.2012.11.012.

Molotch, N. P., and R. C. Bales (2005), Scaling snow observations from the point to t he grid element: Implications for observation network design, *Water Resour. Res.*, *41*, 1–16, doi:10.1029/2005WR004229.

Molotch, N. P., and R. C. Bales (2006), SNOTEL representativeness in the Rio Grande headwaters on the basis of physiographics and remotely sensed snow cover persistence, *Hydrol. Process.*, *20*(September 2005), 723–739, doi:10.1002/hyp.6128.

Oren, R., N. Phillips, B. E. Ewers, D. E. Pataki, and J. P. Megonigal (1999), Sap-flux-scaled transpiration responses to light, vapor pressure deficit, and leaf area reduction in a flooded Taxodium distichum forest., *Tree Physiol.*, *19*(6), 337–347, doi:10.1093/treephys/19.6.337.

Oren, R., J. S. Sperry, B. E. Ewers, D. E. Pataki, N. Phillips, and J. P. Megonigal (2001), Sensitivity of mean canopy stomatal conductance to vapor pressure deficit in a flooded<SMALL> Taxodium distichum</SMALL> L. forest: hydraulic and non-hydraulic effects, *Oecologia*, *126*(1), 21–29, doi:10.1007/s004420000497.

Pister, K. S. J., and L. Doherty (2008), TSMP: Time synchronized mesh protocol, *Proc.Parallel Distrib. Comput. Syst. (PDCS 08)*, 391–398.

Pohl, S., J. Jakob Garvelmann, J. Wawerla, and M. Weiler (2014), Potential of a low-cost sensor network to understand the spatial and temporal dynamics of amountain snow cover Stefan, *Water Resour. Res.*, 2533–2550, doi:10.1002/2013WR014594.Received.

Pomeroy, J., X. Fang, and C. Ellis (2012), Sensitivity of snowmelt hydrology in Marmot Creek, Alberta, to forest cover disturbance, *Hydrol. Process.*, *26*(12), 1891–1904, doi:10.1002/hyp.9248.

Prince, S. D., S. J. Goetz, R. O. Dubayah, K. P. Czajkowski, and M. Thawley (1998), Inference of surface and air temperature, atmospheric precipitable water and vapor pressure deficit using advanced very high-resolution radiometer satellite observations: Comparison with field observations, *J. Hydrol.*, *212–213*(1–4), 230–249, doi:10.1016/S0022-1694(98)00210-8.

Raleigh, M. S., and J. D. Lundquist (2012), Comparing and combining SWE estimates from the SNOW-17 model using PRISM and SWE reconstruction, *Water Resour. Res.*, *48*(November 2011), 1–16, doi:10.1029/2011WR010542.

Refsgaard, J. C. (1997), Parameterisation, calibration and validation of distributed hydrological models, *J. Hydrol.*, *198*(1–4), 69–97, doi:10.1016/S0022-1694(96)03329-X.

Rice, R., and R. C. Bales (2010), Embedded-sensor network design for snow cover measurements around snow pillow and snow course sites in the Sierra Nevada

of California, *Water Resour. Res.*, *46*, 1–13, doi:10.1029/2008WR007318.

Ritsema, C. J., H. Kuipers, L. Kleiboer, E. Van Den Elsen, K. Oostindie, J. G. Wesseling, J. W. Wolthuis, and P. Havinga (2010), A new wireless underground network system for continuous monitoring of soil water contents, *Water Resour. Res.*, *46*(4), 1–9, doi:10.1029/2008WR007071.

Rolland, C. (2003), Spatial and seasonal variations of air temperature lapse rates in alpine regions, *J. Clim.*, *16*(7), 1032–1046, doi:10.1175/1520-0442(2003)016<1032:SASVOA>2.0.CO;2.

Semenova, O., and K. Beven (2015), Barriers to progress in distributed hydrological modelling, *Hydrol. Process.*, *29*(8), 2074–2078, doi:10.1002/hyp.10434.

Sicart, J. E., R. L. H. Essery, J. W. Pomeroy, J. Hardy, T. Link, and D. Marks (2004), A sensitivity study of daytime net radiation during snowmelt to forest canopy and atmospheric conditions, *J. Hydrometeorol.*, *5*, 774–784, doi:10.1175/1525-7541(2004)005<0774:ASSODN>2.0.CO;2.

Simoni, S., S. Padoan, D. F. Nadeau, M. Diebold, A. Porporato, G. Barrenetxea, F. Ingelrest, M. Vetterli, and M. B. Parlange (2011), Hydrologic response of an alpine watershed: Application of a meteorological wireless sensor network to understand streamflow generation, *Water Resour. Res.*, *47*(10), 1–16, doi:10.1029/2011WR010730.

Sturm, M., and C. Benson (2004), Scales of spatial heterogeneity for perennial and seasonal snow layers, *Ann. Glaciol.*, *38*, 253–260, doi:10.3189/172756404781815112.

Trubilowicz, J., K. Cai, and M. Weiler (2010), Viability of motes for hydrological measurement, *Water Resour. Res.*, *46*(4), doi:10.1029/2008WR007046.

Welch, S. C., B. Kerkez, R. C. Bales, S. D. Glaser, K. Rittger, and R. R. Rice (2013), Sensor placement strategies for snow water equivalent (SWE) estimation in the American River basin, *Water Resour. Res.*, *49*(February), 891–903, doi:10.1002/wrcr.20100.

Wood, E. F. et al. (2011), Hyperresolution global land surface modeling: Meeting a grand challenge for monitoring Earth's terrestrial water, *Water Resour. Res.*, *47*(5), 1–10, doi:10.1029/2010WR010090.

Ye, H., J. Cohen, and M. Rawlins (2013), Discrimination of solid from liquid precipitation over northern Eurasia using surface atmospheric conditions, *J. Hydrometeorol.*, *14*(4), 1345–1355.

Yick, J., B. Mukherjee, and D. Ghosal (2008), Wireless sensor network survey, *Comput. Networks*, *52*(12), 2292–2330, doi:10.1016/j.comnet.2008.04.002.

Ziemer, R. R. (1979), Evaporation and transpiration, *Rev. Geophys.*, *17*(6), 1175–1186, doi:10.1029/RG017i006p01175.
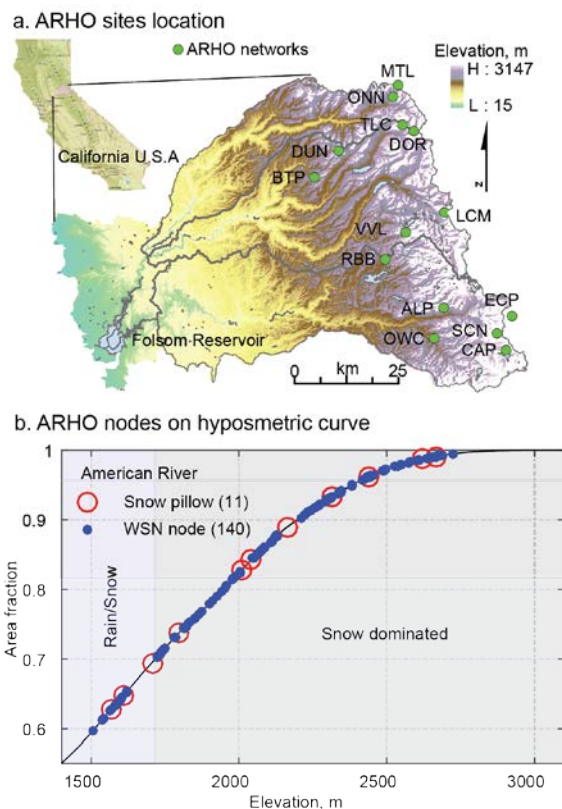
Figure 1. a) Location of American River basin and 14 sensor clusters deployed in the upper part of the basin. b) WSN nodes on hypsometric curve with existing snow pillows.
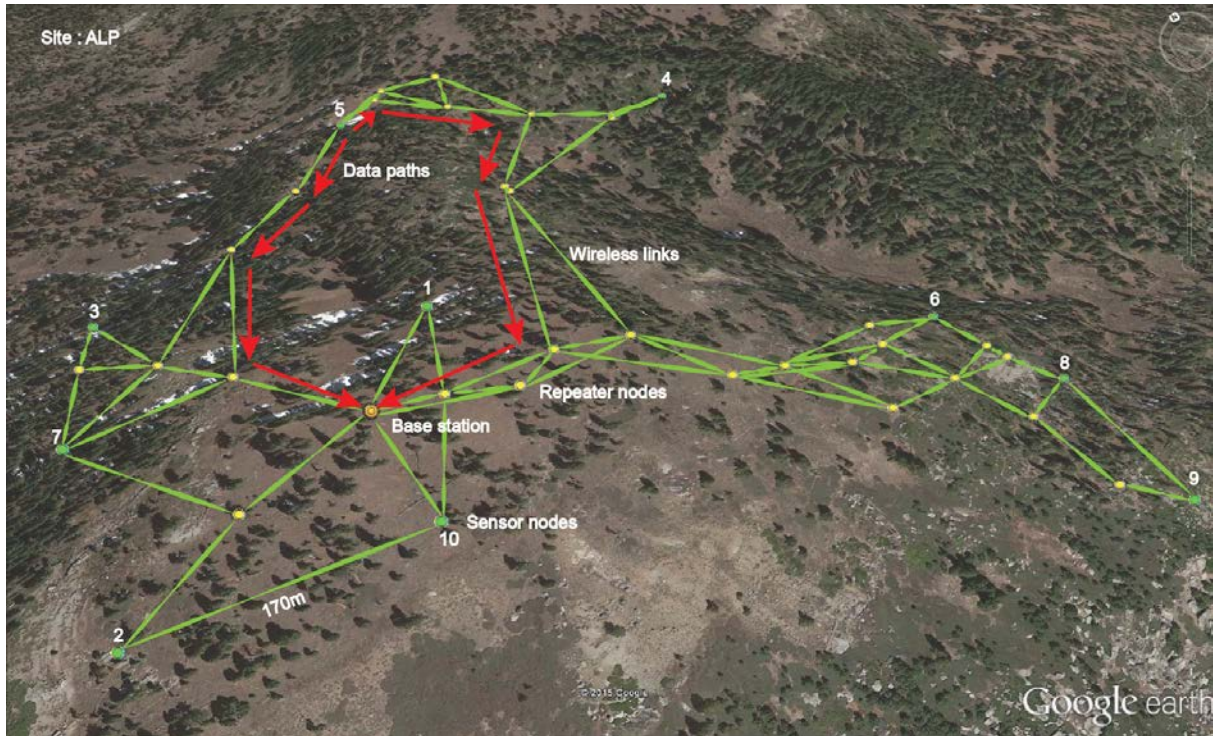
Figure 2. Node layout and steady-state network connections (green lines) at ALP, overlain on Google Map. Sensor nodes are numbered. Two possible paths of data out from sensor node 5 to the base station are marked with red arrows.
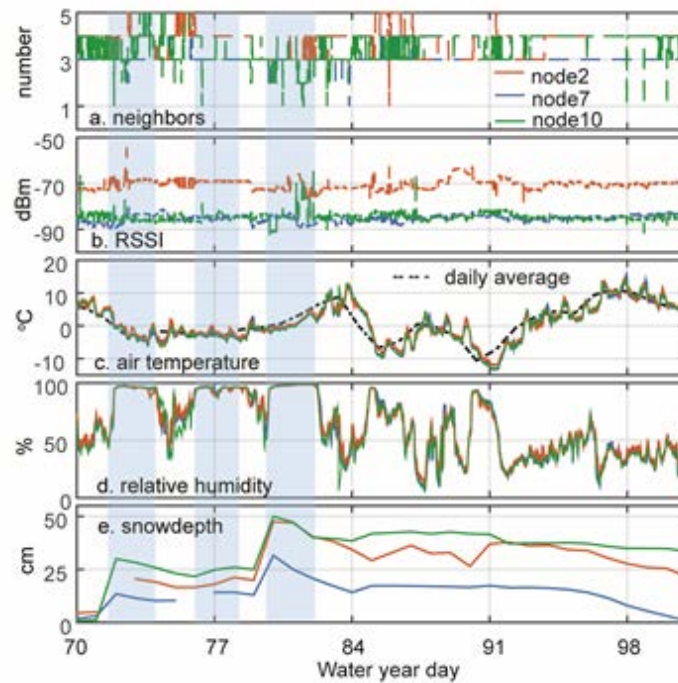

Figure 3. Network performance of sensor nodes 2,7 and 10 at ALP: a) hourly data of network neighbors number, b) the corresponding average RSSI, c) average air temperature, d) hourly average humidity, and e) daily average snow depth. Shaded periods represent precipitation events. For clarity, data from three sensor nodes are presented.
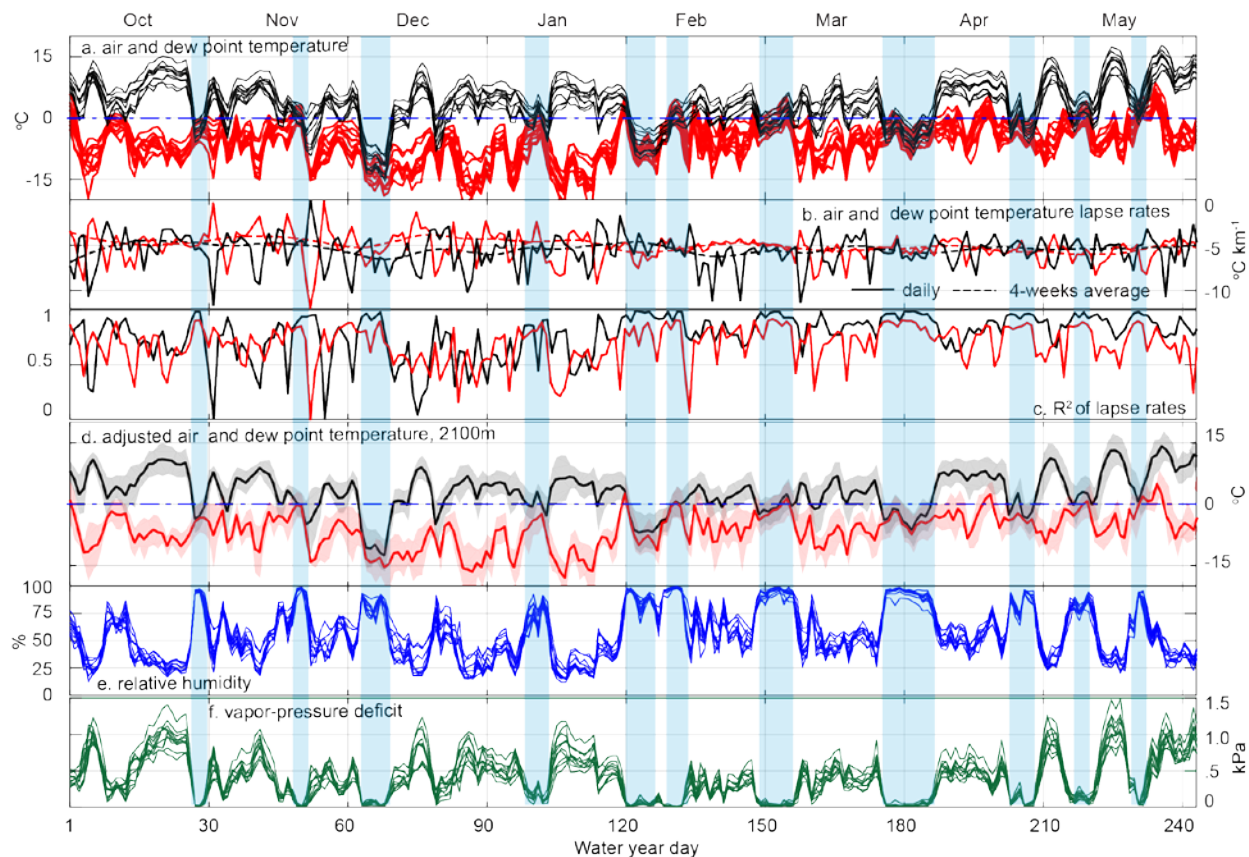
Figure 4. Data from 10 clusters for 8-month period: a) cluster-mean daily averaged air (black traces) and dew-point (red traces) temperature, b) air and dew-point temperature lapse rates, c) R^2 value of daily lapse rates, d) mean (dashed lines) and standard deviation (shading) of site air and dew-point temperatures adjusted to 2100 m elevation using the daily lapse rate, e) mean daily average relative humidity, and f) mean daily vapor-pressure deficit calculated from mean daily temperature and relative humidity of each cluster. Shaded periods represent precipitation events. Data for only 10 of the 14 local clusters are shown, as 4 were brought online after the period reported here.
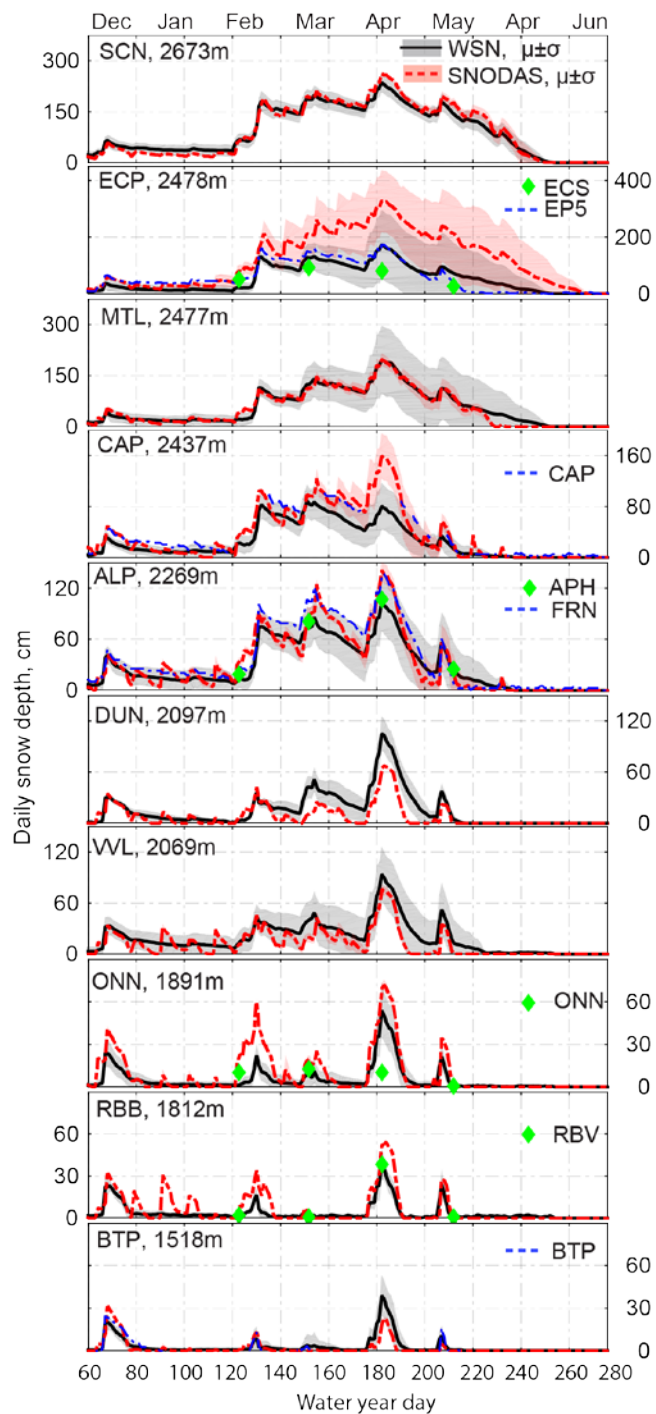
Figure 5. Daily mean (μ) and standard deviation (σ) of snow depth from the WSN clusters and SNODAS, including available operational snow-depth-sensor data (blue dashed), and snow courses (green diamond). See Figure S4 for calculation of SNODAS mean and standard deviation.
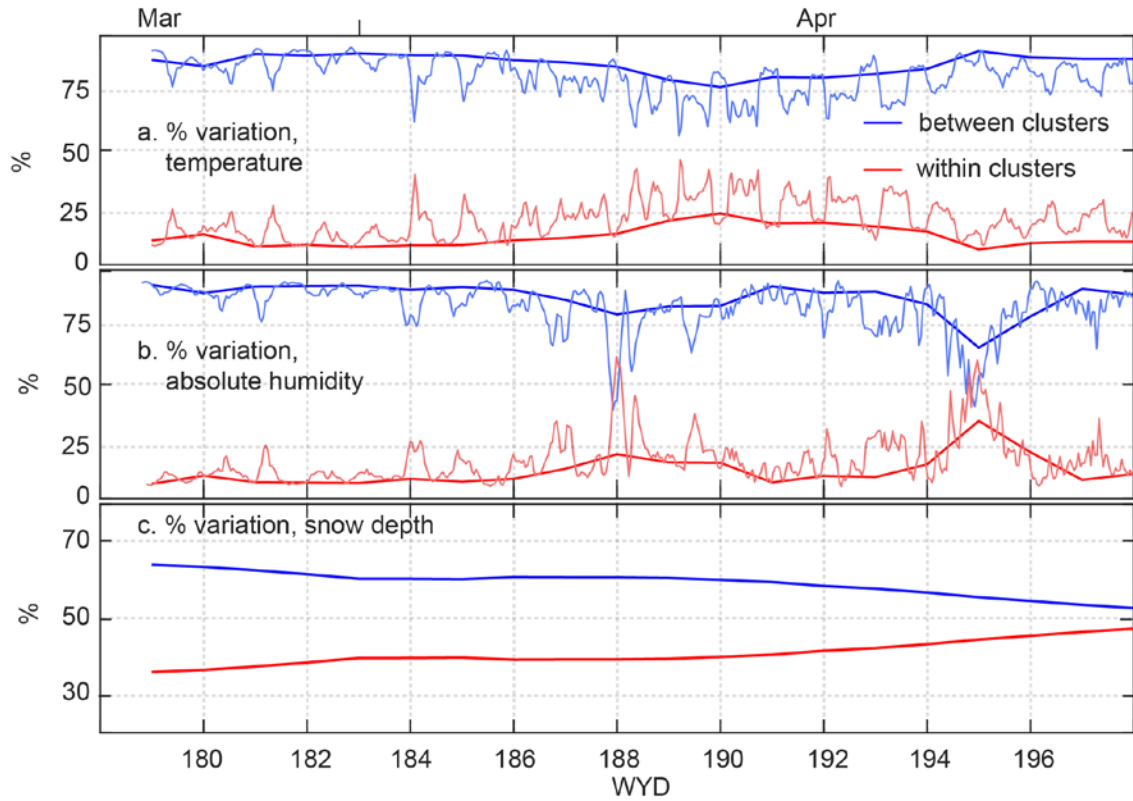
Figure 6. ANOVA results for 20-day period around peak snow accumulation, for between and within-cluster variations in measurements of: a) hourly and daily temperature, b) hourly and daily relative humidity, and c) daily snow depth. See Fig. S7 for data used in the analysis.

Supporting Information for

Technical report: the design and evaluation of a basin-scale wireless sensor network for mountain hydrology

Ziran Zhang[1], Steven D. Glaser[1], Roger C. Bales[1,2], Martha Conklin[2], Robert Rice[2] and Danny G. Marks[3]

[1]Department of Civil and Environmental Engineering, University of California, Berkeley
[2]Sierra Nevada Research Institute and School of Engineering, University of California, Merced
[3]Agricultural Research Service, USDA, Boise, ID

Introduction

This document includes supporting texts and figures and table referenced in the main text.

Text S1

S1.1 Prior WSN deployments for hydrology in remote areas

In 2007, a WSN with a few dozen nodes was deployed to a golf course near Almkerk Netherland to monitor soil moisture. The study claimed to be successful but the description and discussion of the wireless network infrastructure, was very brief [*Ritsema et al.*, 2010]. In 2009, a 12-station, 4-month deployment in a 20-km^2 catchment in the Swiss Alps measured the spatial variability of meteorological forcing, including temperature and precipitation. The study was conducted over a short time period with rather sparsely distributed stations [*Simoni et al.*, 2011]. Recently, densely deployed sensor arrays have been scaled to a size comparable to the mountain areas being studied. Ninety-nine sensor loggers, within three 40-180 km^2 basins, were deployed to monitor snow properties in southern Germany for one winter. The system deployed used data loggers rather than a WSN [*Pohl et al.*, 2014]. In another study, 150 wireless nodes with over 600 soil-moisture sensors were installed in a forest catchment at Westebach, Germany to study the spatiotemporal distribution of soil moisture over complex terrain [*Bogena et al.*, 2010]. The study used a variation of ZigBee motes developed by JenNet Ltd. Over 300 sensors hosted by 60 wireless nodes have been deployed at the Southern Sierra Critical Zone Observatory since 2008 to study heterogeneous interactions of water within the snowpack, canopy and soil influence on the water cycle [*Kerkez et al.*, 2012]. This installation suffered from network optimization issues that limited locations of the sensor nodes, and hardware problems with the cold.

S1.2 Present Solutions for Wireless Sensor Networks – A comparison of existing technologies

Sensor networks are made up of motes. This term, from its definition "a small speck of dust," was coined at UC Berkeley to describe a very small, low-power device that incorporates a radio transceiver, computational power, data storage, and sensors. There are many commercially available motes with many different standards. Different motes were designed for different purposes such as research, education, hobbyists, indoor industrial and outdoor monitoring and control applications. The question is why pick one hardware solution over another? Our primary consideration focuses on how well the networking protocols were implemented to ensure performance and robustness. We also look into the hardware flexibility to satisfy needs for interfacing with different sensors. We focus on the most popular of motes that comply with the IEEE 802.11.15.4 standards for power-savings reasons and availability. Properties and specifications of two main families of motes along with our solutions were investigated.

S1.2.1 Mica-II, Iris, TelosB, Lotus.
Memsic Inc. provides a number of low-power motes (MICA, TelosB, and Lotus) that are 1802.11.5.4 compatible. The MICA and TelosB design goes back almost twenty years to the early UC Berkeley work. The LOTUS mote with a Cortex M3 processor and ZigBee radio provides the most internal memory for the OS and application software among Memsic motes. Several operating systems (RTOS, MoteRunner and TinyOS) can be ported to LOTUS. However, some problems with the network-routing protocol and channel-management protocols remain. Operating on a

single channel makes them vulnerable to network instabilities resulting from signal interference and multi-path effects. The current draw from the LOTUS and MDA300 board is estimated to be around 17 mA at 3V when transmitting. The mote depletes two AA batteries in approximately one month when set to transmit for 3 seconds every 3 min. The data-acquisition board (MDA300) provides seven single-ended and one (multiplexed to four) differential 12-bit ADC channels; digital I/O support is very limited on this board.

S1.2.2 ZigBee and Xbee. ZigBee-based motes represent a popular family of wireless motes that share common communication protocols and specifications (network layer and application layer) by implementing a ZigBee software stack [*ZigBee*, 2009]. In practice ZigBee operates as a star network. Although it is theoretically possible to form a mesh-like network topology, a subset of motes has to be pre-selected and programed as dedicated routing nodes to relay data from the end/leaf node to the coordinator. The RX channel of those router elements has to be constantly powered, which results in high overall energy consumption [*Horvat*, 2012]. ZigBee operates on a single channel, making it difficult to avoid channel interference due to other ISM sources such as WI-FI, and multipath [*Accettura and Piro*, 2014]. ZigBee networks are also not able to meet the reliability and latency requirement for industrial applications [*Gungor and Hancke*, 2009; *Huang et al.*, 2012]. The October 2016 DoS attack on the U.S. web was based on captured zigbee IoT devices, indicating a severe lack of network security.

Digi International maintains a family of motes called Xbee. The XBee 2.4 GHz-band mote has its own proprietary protocol called DigiMesh that suffers from environmental interference and varying effects of multipath because it does not implement channel hopping [*International*, 2009]. In order to achieve low power in a DigiMesh network, the system needs to enter a synchronized sleep mode. Due to the lack of a central network coordinator, a subset of the DigiMesh motes needs to be constantly running to serve as sleep coordinators (i.e., network manager). Those motes continuously broadcast sync message to the surrounding nodes to keep the network assembled, otherwise the message transmitted to a mote during the sleeping period will be permanently lost [*International*, 2009]. Another possible issue for DigiMesh networks in synchronized sleep mode is that when a new mote is added to the network, it needs to be physically near a sleep coordinator to receive a sync message in order to join the network [*Xbee-pro and Rf*, n.d.]. If a node temporarily drops out, it is permanently lost, and an extended trial and error installation is difficult to carry out. Xbees are commonly interfaced with Arduino single-board computers to provide facilities to host sensors, compute, and store data. The Arduino Uno R3, with no external load from sensors and other components, consumes about 40 mA at 5V. The Uno R3 uses a slow and outdated Atmega328P (8-bit/16MHz) microprocessor with a 10-bit analog to digital converter that provides only six analog pins and fourteen digital pins to interface with the sensors and other equipment. Similar issues with power and flexibility can be found with solutions provided by Raspberry Pi, which consumes 700 mA at 5V, making it impractical to operate with a battery. Systems with Arduino and Raspberry Pi are best kept indoors where sufficient power input is provided. They are not recommended for long-term outdoor deployments, as they were designed for hobbyist use.

S1.2.3 Metronome Systems neoMote.
Metronome Systems provides a comprehensive solution for the sensor node called the neoMote, which was developed by UC Berkeley researchers. It combines the DUST Networks Eterna radio module with a Cypress Programmable System on Chip (PSoC5) into a two-chip mote solution. While DUST Network radios provide robust and reliable wireless networking capability, PSoC provides full support to any sensor or control peripheral. The PSoC offers an array of configurable system blocks that can be dynamically added to a project for a particular application. For instance, the board can interface up to 40 analog and/or digital sensors at once, providing all analog and digital signal conditioning and excitation. The PSoC building blocks are available to a drag-and-drop interface and are reprogrammable over the radio. The neoMote provides 3.3, 5, and 12Vdc excitation to sensors. Interfacing with a SD-card slot provides additional storage for data and system parameters. In addition, the board is ultra-low power. Power

consumption is 30 µA, 60 µA in 20-bit A/D mode, with transmission adding 10 mA - two to three orders of magnitude lower than the previous solutions. The network is controlled by a Metronome Systems network manager, which also interfaces the data with the outside world. It is based on a full LINUX computer, while only consuming 50 mA at 5V. It runs a full database and sends the data out through a variety of modems.

DUST Networks, a division of Linear Technology, provides an industrially rated ultra-low power fully meshed wireless networking platform. The dynamic network allows seamless joining and rejoining by any mote or hopper. A few technical details properties of the DUST mote make it superior to other choices. The SmartMesh IP software utilizes time synchronized mesh protocol (TSMP) that maintains complete network synchronization to 10 µs, which minimizes the "on-time" to listen for the beacon. Incorporating Time-Slotted Channel Hopping (**TSCH**) reduces interference within the communication channels through diversity of frequency at which each packet is sent [*Pister and Doherty*, 2008]. Adding diversity to the channel selection reduces the adverse effect of multipath fading in wireless network. The typical duty cycle of the DUST radio module is < 1% while keeping communication reliability 99.999%. The DUST network is unique in that it constantly collects a wide variety of network statistics, which allows for the later optimization of a network.

The Metronome system provides capability for Internet-of-Things functionalities, such that one can deliver programs remotely to sensor nodes to resync real-time clock settings, change firmware, sampling interval, sensor gain, etc.

S2 Physiographic attributes of cluster

Elevations were extracted from a 30-m DEM. Slopes and aspects were calculated using ArcGIS spatial analyst toolbox. Percent canopy cover was extracted from NLCD 2011 data layer [*Jin et al.*, 2013]. Overall, sensor placement reflects a close correspondence between site characteristic of the sensor nodes and the features within the 1-km^2 areas for most of the sites. Mean site elevations range from 1590 to 2680 m, with considerable overlap between some sites (Fig. S1a). Some sites are relatively flat (e.g. CAP) and some on relatively steeper terrain (e.g. MTL, ECP) (Fig. S1b). It was possible to get a range of aspect at most sites, with the notable exception of TLC and CAP (Fig S1c). All other sites have both north and south aspects. Sensor placements capture the range of canopy covers, shown in Fig. S1d.

S3 Details of sensor nodes

Each sensor node (Fig. S3) is equipped with an ultrasonic snow-depth sensor (Judd Communication Depth Sensor) and a temperature/relative humidity sensor (Sensirion SHT-15). A selected subset of the nodes at five of the sites measure soil moisture and soil temperature (Decagon GS3) at depths of 10 and 60 cm. Nine sites include measurements of total incoming solar radiation using an upward-pointing Hukseflux-LP02 pyranometer on a separate mast with a concrete foundation. The solar-radiation sensors at these locations are located in the open, without obstruction by either canopy or the terrain to capture the total available incoming solar irradiance. At nine of the 14 sites, co-located with the clear-sky irradiance, solar radiation is measured in a partially canopy-covered location, providing representative solar irradiance-measurements underneath the canopy structure. The accuracy and the resolution of the sensors is described in Table S2. It should be noted that our wireless nodes are not limited to these sensors, which were chosen based on past performance, cost and consistency with other networks.

Table S1. Equipment installed for sites

Site	Name	Lat, Lon	Temperature, relative-humidity	Snow depth	Soil water	Solar radiation
SCN	Schneiders	38.745,-120.067	10	10	10	2
ECP	Echo Peak	38.848,-120.079	10	10	0	2
MTL	Mt. Lincoln	39.287,-120.328	10	10	0	1
CAP	Caples Lake	38.711,-120.042	10	10	0	2
LCM	Lost Corner	39.017,-120.216	10	10	0	0
ALP	Alpha	38.804,-120.216	10	10	10	1
DUN	Duncan Peak	39.154,-120.510	11	11	10	2
VVL	Van Vleck	38.944,-120.306	10	10	10	1
DOR	Dolly Rice	39.149,-120.369	10	10	0	0
ONN	Onion Creek	39.274,-120.356	10	10	0	2
RBB	Robb Saddle	38.912,-120.379	10	10	0	2
TLC	Talbot Camp	38.944,-120.306	10	10	0	0
OWC	Owens Camp	38.736,-120.241	10	10	0	0
BTP	Bear Trap	39.095,-120.577	10	10	0	0

Table S2. Sensors used for field monitoring

Sensirion SHT-15 temperature/relative humidity sensor
- 2% rH accuracy
- 12-bit digital resolution rH
- 0.3°C temperature accuracy
- 14-bit temperature resolution
- factory calibration
- digital interface

Judd Ultrasonic Depth Sensor
- 0.5 to 10 m range
- 0.4% distance to target distance accuracy
- digital or analog output
- calibrated in the field

Decagon GS3 Soil Volumetric Water content and Temperature Sensor
- $\pm$ 0.03 m^3/m^3 ($\pm$ 3% VWC) volumetric water content accuracy
- complex resistivity-type measurement technique
- $\pm$ 1°C soil temperature accuracy
- 3.6V TTL output

Hukseflux LP02 Pyranometer
- second class specifications
- 285 to 3000 x 10^{-9} m spectral range
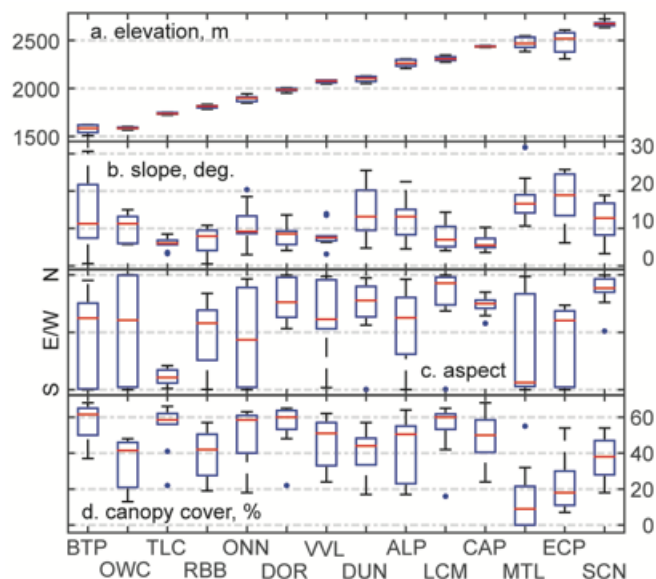- 15 x 10^{-6} V/(W/m^2) sensitivity

Figure S1. Characteristics of individual sites, arranged from lowest to highest elevation. See Table S1 for site abbreviations: a) elevation in m, b) slope (°), c) aspect (S to N) and d) canopy cover (%). The central red mark is the median, the edges of the box are the 25th and 75th percentiles, the whiskers extended to the extreme points not considered outliers, and the blue dots are the outliers.
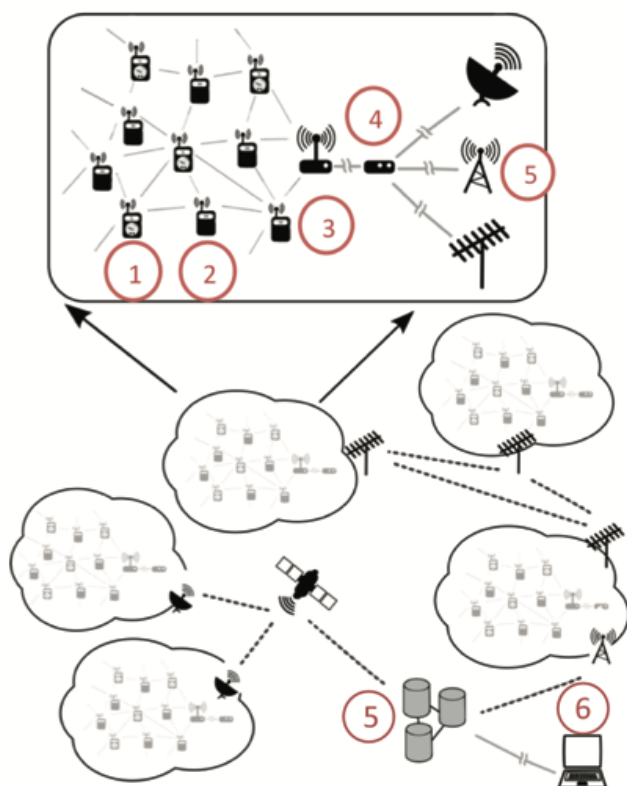
Figure S2. American River basin system hierarchy: local WSN clusters connect to central server through data links provide by cell phone or satellite modems: (1) wireless sensor nodes (a neoMote, sensors and external power infrastructure); (2) repeater nodes; (3) Metronome network manager/base station; (4) external connection to the Internet; (5) central-site data server; and (6) real-time visualization engine and data portal.
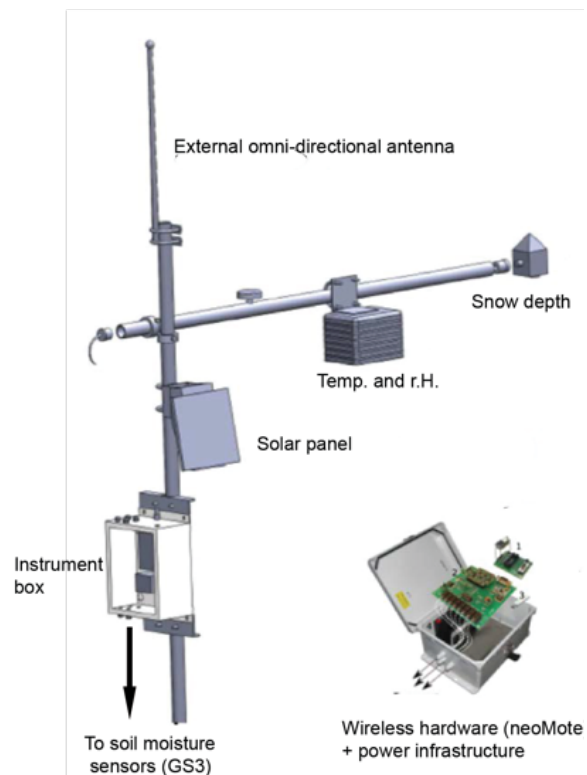

Figure S3. Sensor node detail. The 4.5 m vertical mast is bolted to a U-channel driven into the ground. Sensors are either buried under ground or mounted on a 1.2-m long cross arm 4 m above ground.
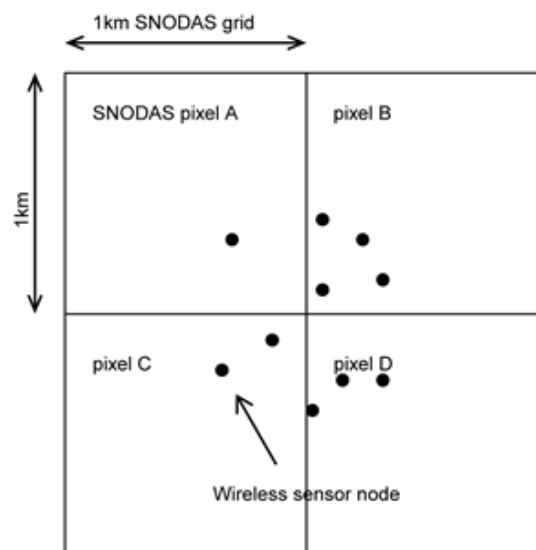
Figure S4. Illustration of how a weighted average of SNODAS SWE data were calculated for each local cluster, for comparison with WSN data. For SNODAS data gridded at 1-km spatial resolution, pixels containing nodes for each local cluster were extracted and averaged for that local cluster. In the example shown, the SNODAS mean of this site was calculated as (A+4B+2C+3D)/10.
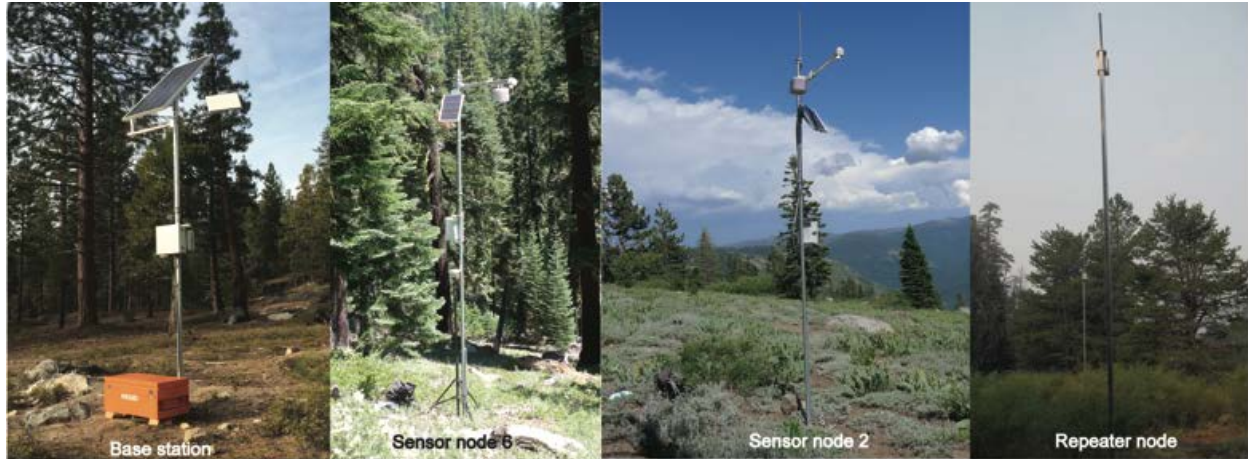
Figure S5. Photos of base station, two sensor nodes, and a repeater node at ALP.
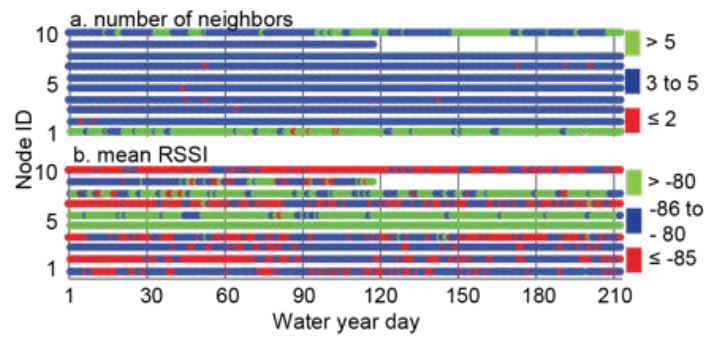

Figure S6. Average daily network performance of sensor nodes at Alp for seven-month period. Top panel shows number of network neighbors for each of the 10 sensor nodes, and bottom panel is the average received signal strength indicator (RSSI) for each sensor node. A white gap indicates no communication. The data-stream gap for node 9 in January 2015 was due to a non-network related hardware failure.
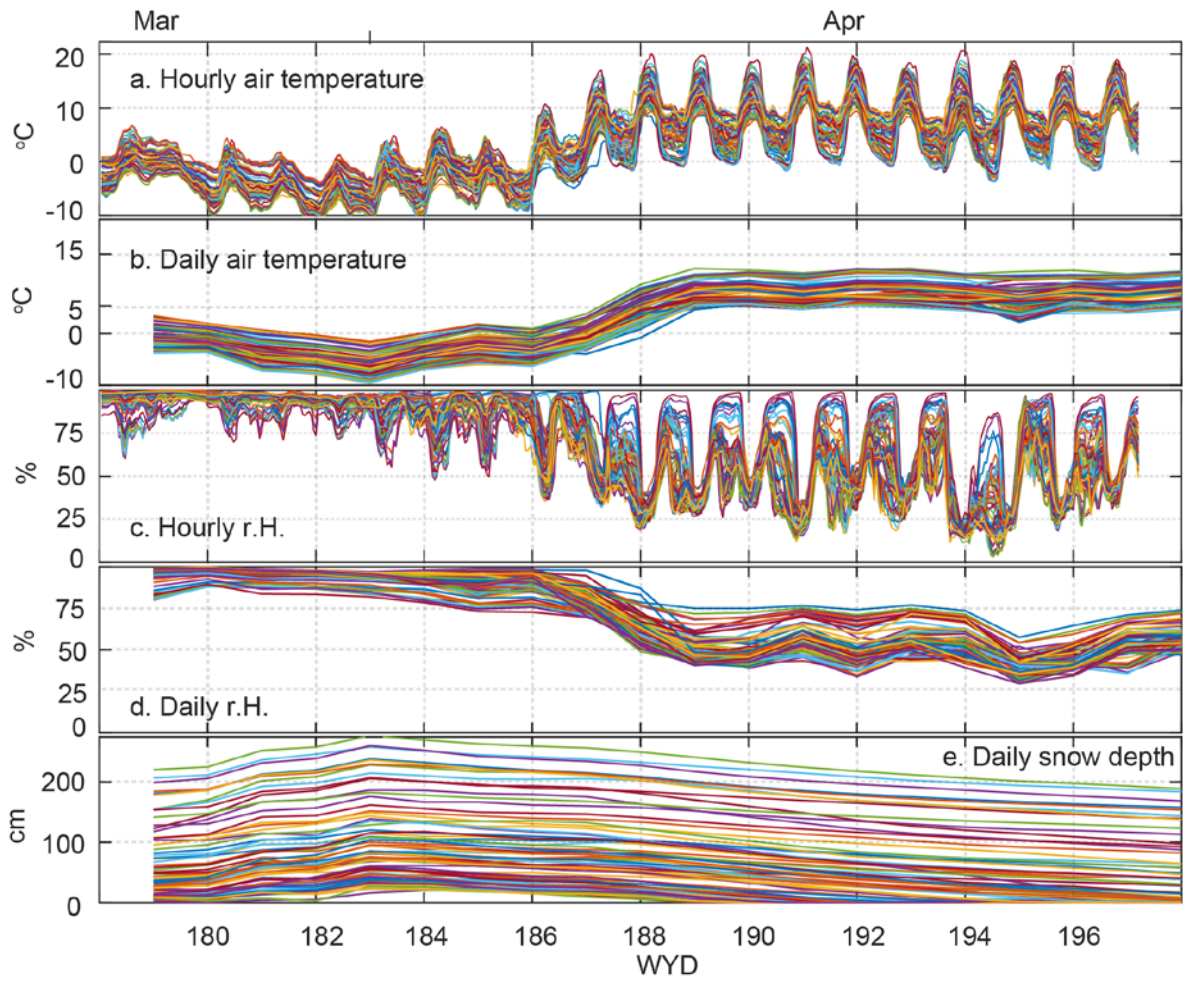
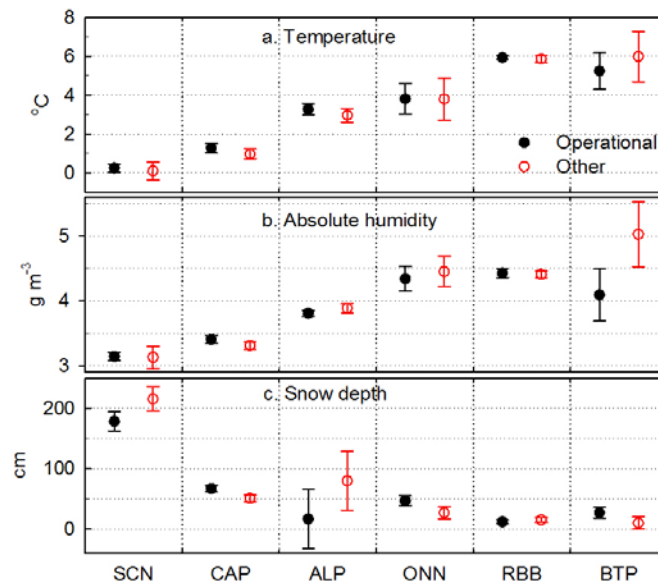**Figure S7. Data used in ANOVA analysis (Figure 6). From all clusters, all nodes.**

Figure S8. Comparison of a) temperature, b) absolute humidity and snow depth for 6 local clusters with at least 8 nodes reporting for the 20-day period (water year days 179-199) around peak accumulation. Operational refers to the subset of nodes that have landscape attributes like those of co-located operational sensors (flat, open); and other refers to other sensors in the local cluster that have some degree of slope and canopy cover.